Sensors & Diagnostics

COMMUNICATION

View Article Online
View Journal | View Issue

Cite this: *Sens. Diagn.*, 2023, **2**, 1176

Received 23rd April 2023,
Accepted 15th June 2023

DOI: 10.1039/d3sd00097d

rsc.li/sensors

An exfoliated redox active imide covalent organic framework for metal free hydrogen gas sensing†

Nany Thokala,[a] Kiran Vankayala,[b] Asmita Dileep Gaonkar,[b] Ganga Periyasamy,[c] Kashifa Fazl-Ur-Rahman,[c] Krishnaveni Valle,[a] Marilyn Esclance DMello,[d] Keloth Basavaiah[a] and Suresh Babu Kalidindi *[e]

A two dimensional (2D) redox active donor–acceptor COF made of triphenylamine (TPA) and naphthalenediimide (NDI) acted as an efficient hydrogen chemisresistor and performed better than traditional metal oxides. Calculations have shown that the charge transfer interaction between H_2 and an NDI linker through a carbonyl functionality enables a change in the resistance of the material upon exposure to H_2 gas.

Covalent organic frameworks (COFs) are a versatile class of crystalline porous organic polymers which have been drawing the interest of researchers from a wide range of areas since their discovery in 2005 by Yaghi *et al.*[1] COFs are acclaimed for multiple applications like gas storage,[2] supports for catalysts,[3] adsorption and separation of gases,[4] energy storage,[5] opto-electronics[6] and very recently in sensing.[7] Two dimensional (2D) COFs in particular have gained much attention due to their interesting electronic and optical properties because of their extended in-plane π-conjugation. Uniform distribution of active functionalities over these extended frameworks increases the analyte interaction during sensing applications and ensures proper signal transduction.[8] Although COFs have been widely studied as sensors based on fluorescence and absorption mechanisms,[9,10] COF based chemiresistive sensors are few.

Sensors based on the measurement of change in the resistance upon exposure to analyte gas, *i.e.* chemiresistors, are much simpler, and miniaturization can be done quite easily.[11] In this direction, Q. H. Wang *et al.* have reported for the first time the use of COFs for the detection of NH_3 using covalent triazine framework (CTF)[12a] based COFs. Subsequently, COFs containing imine,[12b] heptazine[12c] and truxene[12d] linkages are used for sensing NH_3, NO_2, humidity, *etc.* Although these latest studies highlight the potential of COFs for chemisresitive gas sensing, looking at the diverse COFs available in the literature, the area is still in an early stage (only 8 studies so far, to the best of our knowledge).[12e–h] For instance, redox active COFs have not been explored in this direction. Also, neat COF based H_2 sensors are yet to be developed. H_2 is an emerging alternative source of clean energy and at the same time, it is highly flammable at concentrations above 4% in air.[13] Pd based chemisresistive H_2 sensors have been widely reported due to good affinity of Pd towards H_2. Although most of the Pd based sensors exhibit quick response, the recovery times are not appreciable.[14] Further, Pd is an expensive metal, which warrants the development of cost-effective H_2 sensors that are devoid of expensive metals like Pd, Pt, *etc.*

In the present study, a chemiresistive sensing device is fabricated using a colloidal dispersion of an exfoliated redox active COF constructed from naphthalene-1,4,5,8-tetracaboxylic dianhydride (NDA) and tris(4 aminophenyl) amine (TAPA), NDA–TAPA COF (NT COF) as a sensing element. The NT COF is a 2D crystalline porous polyarylimide well known for its high redox activity.[15a] The regular arrangement of electron donor units (triphenylamine, TPA) and electron acceptor units (naphthalenediimide, NDI) in the framework makes this material attractive for electronic applications.[15b] Notably, this COF with robust cyclic imide linkages and strong π–π conjugation has high thermal and chemical stability.[15c] Keeping its structural and intrinsic properties in mind, we reasoned that this COF could be a suitable candidate for the chemiresistive detection of reducing gases like H_2.

The NT COF was synthesised by a solvothermal method where the imidization of precursors, namely naphthalene-

[a] *Department of Chemistry, Andhra University, Visakhapatnam, 530003, India*
[b] *Department of Chemistry, Birla Institute of Technology and Science, Pilani, K. K. Birla Goa campus, Goa, 403726, India*
[c] *Department of Chemistry, Bangalore University, Bangalore-56, India*
[d] *Materials Science Division, Poornaprajna Institute of Scientific Research, Bidalur post, Devanahalli, Bengaluru, 562 110, India*
[e] *Department of Chemistry, Central Tribal University of Andhra Pradesh, AU PG Centre, Vizianagaram, 535003, India. E-mail: ksureshu@gmail.com, suresh.babu@ctuap.ac.in*

† Electronic supplementary information (ESI) available. See DOI: https://doi.org/10.1039/d3sd00097d

1,4,5,8-tetracarboxylic dianhydride (0.15 mmol) and tris(4 aminophenyl)amine linker (0.10 mmol), was carried out under controlled conditions following the literature procedure[16] (Fig. 1a). Bulk COF powders typically consist of insoluble microcrystalline aggregated particles that are difficult to disperse in a suitable solvent, leading to challenges in processability of bulk COFs, which in turn becomes a critical aspect in electronic device fabrication.[17] Since COF layers are held together by weak forces, they can be brought into solvents by using apt exfoliation methods. Among various reported exfoliation methods,[18] we employed the acid exfoliation method for delaminating the layers of the NT COF, to obtain the exfoliated NT COF hitherto named as eNT COF. The acid exfoliation procedure involves vigorous stirring of the NT COF in a mixture of anhydrous acetonitrile, anhydrous tetrahydrofuran and trifluoroacetic acid (7 : 3 : 2 ratio). A similar methodology was previously used for the exfoliation of imine based COFs.[19]

The PXRD pattern of the eNT COF suggests that the crystal structure of the bulk 2D COF is majorly intact even after exfoliation, suggesting insignificant structural rearrangements.[20] However, a new reflection at 2θ = 28.5° corresponding to an interlayer distance of 0.31 nm is observed which probably appeared due to the restacking of layers during exfoliation[21] (Fig. 1b). In the FT-IR spectra, the retention of peaks at 1714, 1668 and 1352 cm^{-1} confirms the intactness of the imide linkage in the eNT COF[22] in comparison with the bulk NT COF (Fig. 1c). We also noticed the appearance of new peaks at 1640 and 3435 cm^{-1} which can be attributed to the conversion of some of the imide linkages in the NT COF to amic acid linkages during exfoliation (Fig. S6 in the ESI†).[23] Nevertheless, Raman spectral bands observed in the case of NT COF remain unchanged in eNT COF, suggesting the intactness of the COF structure even after exfoliation (Fig. S7 in the ESI†). The eNT COF maintained an uninterrupted π-conjugation in the framework similar to the parent material. The UV-visible spectrum of eNT COF showed a broad absorption peak that extended up to 800 nm, similar to the bulk NT COF (Fig. S8 in the ESI†), whereas the absorption by the monomers is largely restricted to 250–400 nm range. This indicates the presence of delocalized π-conjugation in eNT COF (Fig. 1e). The fast Fourier transform (FFT) image generated from the HRTEM data shows diffraction spots corresponding to lattice spacings of 0.39 and 0.31 nm. The 0.39 nm lattice spacing matches with d_{001} of NT COF, whereas 0.31 nm (2θ = 28.5) is assigned to a new interlayer distance that has been created due to acid exfoliation (Fig. 1d). Atomic force microscopy (AFM) images reveal the thickness of nanosheets in the range of 17 to 20 nm which supports the exfoliation of the bulk

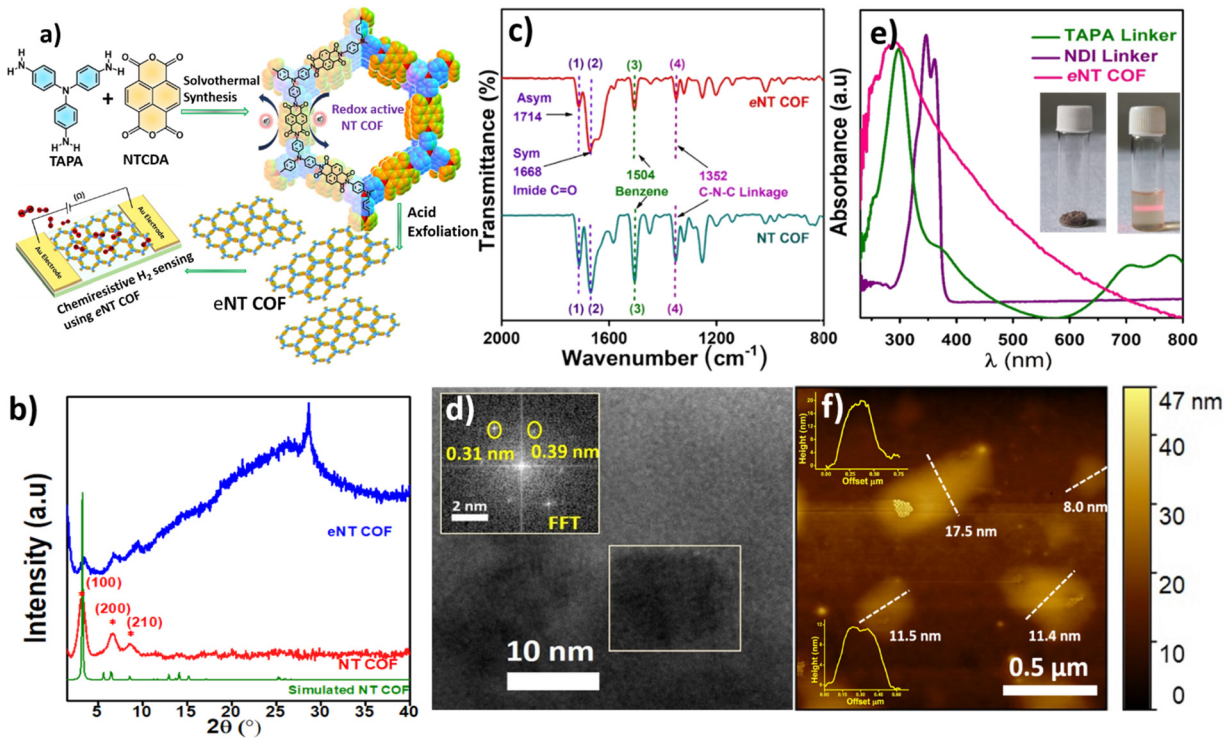

Fig. 1 a) Schematic illustration of the structure of the NT COF showing the solvothermal synthesis of the NT COF, acid exfoliation of the NT COF (eNT COF) and chemiresistive hydrogen gas sensing device using eNT COF. b) Powder X-ray diffraction (PXRD) patterns of bulk and eNT COFs. c) Fourier transform infrared spectroscopy (FTIR) comparison spectra of bulk and eNT COFs. d) High-resolution TEM (HRTEM) image of eNT COF (inset shows the fast Fourier transform (FFT) image of the selected area). e) UV-visible spectra of monomers and eNT COF with the inset showing digital photographs of bulk NT COF powder and the Tyndall effect in the colloidal dispersion of eNT COF. f) Atomic force microscopy image of eNT COF indicating thickness; insets show the height profiles for a few grains.

COF to few-layer-thick 2D sheets (~40–50 layers) (insets of Fig. 1f show the height profiles of a few grains). Further, FESEM analysis of the drop-cast colloidal dispersions of eNT COF revealed interconnected flattened flakes (Fig. S5 in the ESI†). The solid state CP-MAS ^{13}C NMR spectrum of eNT COF exhibited a characteristic resonance at 163 ppm corresponding to the carbonyl carbon of the imide ring and additional signals observed at 110 to 150 ppm represent the aromatic carbon backbone (Fig. S9 in the ESI†). The ^{13}C NMR spectrum of eNT COF was found to be consistent with those in earlier reports.[22]

To assess H_2 sensing functionalities of the COF materials, interdigitated Au electrodes (IDEs) having 10 pairs of fingers with a 100 μm spacing were used. The sensing experiments were carried out using a home built setup described in Scheme S1.† The bulk NT COF was suspended in ethanol and drop-cast on an IDE at 60 °C under a N_2 flow (500 sccm) which is heated to 80 °C in order to obtain an active layer/film. Initially, the bulk NT COF was exposed to 1% H_2 at 200 °C and 1 V bias was applied across the electrodes. The bulk COF did not respond to H_2 gas, rather it exhibited a noisy baseline (Fig. S16 in the ESI†). Bulk COF powders possess voids or huge grain boundaries between the particles. This can block electron mobility and hinder signal transduction.[17] Under similar conditions, IDE devices consisting of eNT COF as the active component (Fig. 2a, inset) exhibit a clear response to H_2 gas with a sensing response of 30.7 ± 0.26% with 4.5 ± 0.6 s and 3.9 ± 0.3 s response and recovery times respectively (Fig. 2a). The exfoliation provides good contact between COF particles and easy access to the active sites which facilitates the interaction of analyte gas with the COF in a favourable manner.[24] Fig. 2b shows the response–recovery cycle profile of the eNT COF-based sensor recorded at 200 °C and 1 V bias upon exposure to 1% H_2 gas. The sensor is found to be recyclable at this temperature with >99% recovery (Fig. S15, Table S4 in the ESI†). Further, to evaluate the characteristics of the present sensor, studies are carried out at temperatures ranging from 80 °C to 250 °C. At 80 °C, the percentage response (R%) is measured to be 60.0 with response and recovery times 4.5 ± 0.6 s and 3.9 ± 0.3 s respectively (Fig. S17 in the ESI†). With the increase in temperature, we noticed less noise and more stable baselines owing to the increase of electron density in the conduction band. Later, the temperature is increased further from 100 °C to 250 °C with an interval of 50 °C. The sensing data obtained at 100 °C and 150 °C are given in Fig. S18 and S19, and Table S5 and S6 in the ESI† respectively. At 200 °C, the SNR improved by 7 fold as evident from Fig. 3a. However, a further increase in temperature to 250 °C (Fig. S21 in the ESI†) resulted in the reduction of both R% and SNR values. Thus, 200 °C is found to be the optimum temperature for eNT COF that would exhibit better performance. The sensor was exposed to different concentrations of H_2 gas ranging from 1 to 0.2% at 200 °C (Fig. 2c). A good linear relationship was obtained between R% and concentration of H_2 with R^2 = 0.97 (Fig. 2d). The R% increases from 7.4 ± 0.25 to 30.7 ± 0.26 with the increase in concentration of H_2 from 0.2 to 1%. It can be noted that there is only a marginal increase in the response time from 3.2 ± 0.8 s to 4.5 ± 0.6 s and recovery time from 3.7± 1.5 s to 3.9 ± 0.3 s with the increase in temperature. The limit of detection (LOD) of eNT COF is found to be 0.14% (section S8 in the ESI†). The overall sensing data are given at 200 °C in Fig. S20 and Table S7 in the ESI.† The performance of the eNT COF chemiresistor for H_2 sensing is superior to those of many traditional metal oxide (SnO_2, ZnO, WO_3, *etc.*)[25] based sensors as shown in Table S2 in ESI.† Further, PXRD, FT-IR, and Raman spectra, and UV-visible spectral data for eNT COF after H_2 sensing were collected (Fig. S10 in the ESI†). These data ascertain insignificant changes in the structure of eNT COF after H_2 sensing, suggesting the robustness of eNT-COF to realize durable sensors.

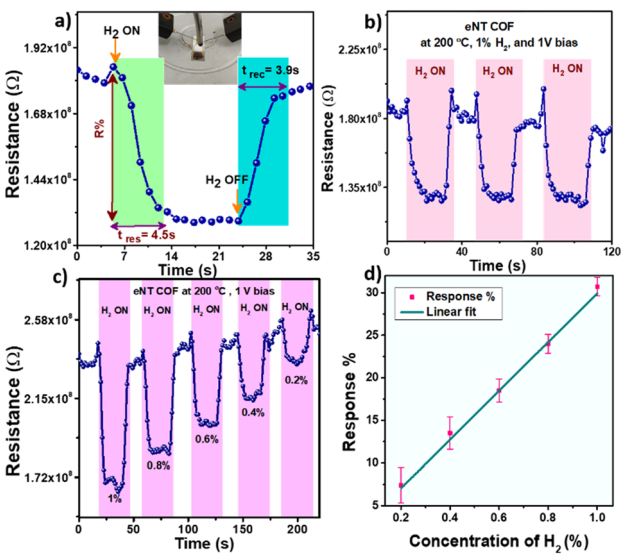

Fig. 2 Dynamic H_2 gas sensing performance of eNT COF. a) H_2 gas sensing curve of eNT COF at an optimum temperature of 200 °C; the inset shows the sensing device in a probe chamber. b) Response and recovery curve of eNT COF at optimum temperature with 1% H_2 concentration. c) Concentration effect of H_2 from 1 to 0.2% at 200 °C. d) Response % *versus* concentration plot of eNT COF.

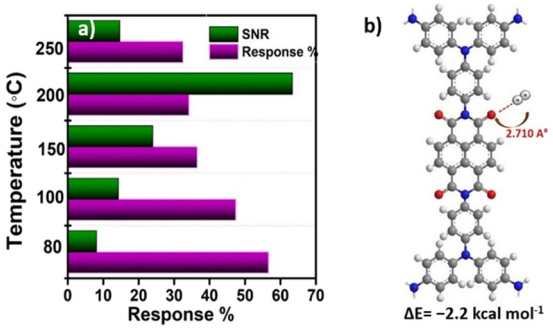

Fig. 3 a) Comparison of response % *versus* signal-to-noise ratio of the eNT COF gas sensor at different temperatures. b) Molecular electrostatic potential plot of the optimized binding site.

To obtain an insight into the sensing mechanism of eNT COF, DFT calculations are carried out by considering the structural models of the monomer using the Gaussian 09 package (computational details are given in the ESI†). The HOMO is localised on the TPA unit (donor) and LUMO on the NDI unit (acceptor).[16] Further, the calculations suggested electrostatic interactions primarily between H_2 and the carbonyl oxygen atoms (with a distance of 2.710 Å) of the NDI linker with an associated binding energy of −2.2 kcal mol^{-1} (Fig. 3b). The computed partial Mulliken charge shows the charge transfer from an H_2 molecule to an oxygen atom of NDI (Table S3 in the ESI†). Notably, when the model system was subjected to a uniform electric field of 0.001 V $Å^{-1}$, the relative negative charge on the carbonyl oxygen atom of NDI increased. As a result, the electrostatic interaction between oxygen and H_2 increased, by ~0.5 kcal mol^{-1}. Nevertheless, the interactions between the framework and H_2 are reversible, and the charge transfer direction supports the observed negative sigmoidal response.

Overall, the first COF based H_2 sensor with attractive gas sensing characteristics has been successfully developed using a structurally rich redox active NT COF. The bulk NT COF powder has been converted into a colloidal suspension using an acid exfoliation method in order to increase the processability for device fabrication. Although eNT COF could sense H_2 at 80 °C, a good trade-off between the signal-to-noise ratio and response (R%: 30.7 ± 0.26, SNR = 65) was achieved at 200 °C. The performance noted for eNT COF is superior to those for several widely studied metal oxides. DFT calculations have suggested that a carbonyl oxygen of the NDI linker interacts reversibly with H_2 through a charge transfer from H_2 to the carbonyl oxygen of NDI. This was also supported by the Mulliken charge analysis. Overall, the study demonstrates the first COF based H_2 sensor and expands the scope of applicability of COFs for chemiresistive sensing.

Author contributions

Conceptualization: SBK and NT. Methodology: SBK, NT, KV, GP, KFUR, ADG, VK, KB and MED. Writing original draft: SBK, NT, KV and GP. Visualization: SBK. Supervision: SBK. Funding acquisition: SBK. The manuscript was written through contributions of all authors. All authors have given approval to the final version of the manuscript.

Conflicts of interest

There are no conflicts to declare.

Acknowledgements

SBK acknowledges Science and Engineering Research Board (SERB)-Department of Science and Technology (DST), Govt. of India for funding under core research grant (CRG/2019/003925). Central sophisticated instrumentation facility (CSIF), BITS Pilani, KK Birla Goa campus is acknowledged for research facilities (SEM, XRD, Raman).

Notes and references

1 (*a*) A. P. Côté, A. I. Benin, N. W. Ockwig, M. O'Keeffe, A. J. Matzger and O. M. Yaghi, *Science*, 2005, **310**, 1166–1170; (*b*) H. L. Nguyen, *Chem. Sci.*, 2021, **12**, 8632–8647; (*c*) Y. Li, W. Chen, G. Xing, D. Jiang and L. Chen, *Chem. Soc. Rev.*, 2020, **49**, 2852–2868.
2 H. Furukawa and O. M. Yaghi, *J. Am. Chem. Soc.*, 2009, **131**, 8875–8883.
3 H. Xu, J. Gao and D. Jiang, *Nat. Chem.*, 2015, **7**, 905–912.
4 C. X. Yang, C. Liu, Y. M. Cao and X. P. Yan, *Chem. Commun.*, 2015, **51**, 12254–12257.
5 D. G. Wang, T. Qiu, W. Guo, Z. Liang, H. Tabassum, D. Xia and R. Zou, *Energy Environ. Sci.*, 2021, **14**, 688–728.
6 D. A. Vazquez-Molina, G. S. Mohammad-Pour, C. Lee, M. W. Logan, X. Duan, J. K. Harper and F. J. Uribe-Romo, *J. Am. Chem. Soc.*, 2016, **138**, 9767–9770.
7 C. Zhao, L. Zhang, Q. Wang, L. Zhang, P. Zhu, J. Yu and Y. Zhang, *ACS Appl. Mater. Interfaces*, 2021, **13**, 20397–20404.
8 D. Jiang, *Chem*, 2020, **6**, 2461–2483.
9 S. Y. Ding, M. Dong, Y. W. Wang, Y. T. Chen, H. Z. Wang, C. Y. Su and W. Wang, *J. Am. Chem. Soc.*, 2016, **138**, 3031–3037.
10 Z. Li, Y. Zhang, H. Xia, Y. Mu and X. Liu, *Chem. Commun.*, 2016, **52**, 6613–6616.
11 M. E. DMello, N. G. Sundaram, A. Singh, A. K. Singh and S. B. Kalidindi, *Chem. Commun.*, 2019, **55**, 349–352.
12 (*a*) L. M. Tao, F. Niu, D. Zhang, T. M. Wang and Q. H. Wang, *New J. Chem.*, 2014, **38**, 2774–2777; (*b*) F. Niu, Z. W. Shao, J. L. Zhu, L. M. Tao and Y. Ding, *J. Mater. Chem. C*, 2021, **9**, 8562–8569; (*c*) N. Sharma, N. Sharma, P. Srinivasan, S. Kumar, J. B. Balaguru Rayappan and K. Kailasam, *J. Mater. Chem. A*, 2018, **6**, 18389–18395; (*d*) H. Singh, V. K. Tomer, N. Jena, I. Bala, N. Sharma, D. Nepak, A. De Sarkar, K. Kailasam and S. K. Pal, *J. Mater. Chem. A*, 2017, **5**, 21820–21827; (*e*) W. C. Ko, M. S. Kim, Y. J. Kwon, J. Jeong, W. R. Kim, H. Choi, J. K. Park and Y. K. Jeong, *J. Mater. Chem. A*, 2020, **8**, 19246–19253; (*f*) F. Niu, Z. W. Shao, L. M. Tao and Y. Ding, *Sens. Actuators, B*, 2020, **321**, 128513; (*g*) K. Yang, W. Yuan, Z. Hua, Y. Tang, F. Yin and D. Xia, *ACS Appl. Mater. Interfaces*, 2020, **12**, 3919–3927; (*h*) Z. Meng, R. M. Stolz and K. A. Mirica, *J. Am. Chem. Soc.*, 2019, **141**, 11929–11937.
13 W. T. Koo, H. J. Cho, D. H. Kim, Y. H. Kim, H. Shin, R. M. Penner and I. D. Kim, *ACS Nano*, 2020, **14**, 14284–14322.
14 W. Zeng, T. Liu, D. Liu and E. Han, *Sens. Actuators, B*, 2011, **160**, 455–462.
15 (*a*) G. Wang, N. Chandrasekhar, B. P. Biswal, D. Becker, S. Paasch, E. Brunner, M. Addicoat, M. Yu, R. Berger and X. Feng, *Adv. Mater.*, 2019, **31**, 1–6; (*b*) B. Sun, X. Li, T. Feng, S. Cai, T. Chen, C. Zhu, J. Zhang, D. Wang and Y. Liu, *ACS*

Appl. Mater. Interfaces, 2020, **12**, 51837–51845; (*c*) M. Yu, N. Chandrasekhar, R. K. M. Raghupathy, K. H. Ly, H. Zhang, E. Dmitrieva, C. Liang, X. Lu, T. D. Kühne, H. Mirhosseini, I. M. Weidinger and X. Feng, *J. Am. Chem. Soc.*, 2020, **142**, 19570–19578.

16 J. Lv, Y. X. Tan, J. Xie, R. Yang, M. Yu, S. Sun, M. De Li, D. Yuan and Y. Wang, *Angew. Chem., Int. Ed.*, 2018, **57**, 12716–12720.

17 X. Zhao, P. Pachfule and A. Thomas, *Chem. Soc. Rev.*, 2021, **50**, 6871–6913.

18 Y. Tao, W. Ji, X. Ding and B. H. Han, *J. Mater. Chem. A*, 2021, **9**, 7336–7365.

19 D. W. Burke, C. Sun, I. Castano, N. C. Flanders, A. M. Evans, E. Vitaku, D. C. McLeod, R. H. Lambeth, L. X. Chen, N. C. Gianneschi and W. R. Dichtel, *Angew. Chem., Int. Ed.*, 2020, **59**, 5165–5171.

20 L. Jiang, Y. Tian, T. Sun, Y. Zhu, H. Ren, X. Zou, Y. Ma, K. R. Meihaus, J. R. Long and G. Zhu, *J. Am. Chem. Soc.*, 2018, **140**, 15724–15730.

21 C. Kang, Z. Zhang, V. Wee, A. K. Usadi, C. David, L. S. Baugh, S. Wang, Y. Wang and D. Zhao, *J. Am. Chem. Soc.*, 2020, **142**, 12995–13002.

22 G. Li and Z. Wang, *J. Phys. Chem. C*, 2013, **117**, 24428–24437.

23 J.-W. Lee, G. Barin, G. W. Peterson, J. Xu, K. A. Colwell and J. R. Long, *ACS Appl. Mater. Interfaces*, 2017, **9**, 33504–33510.

24 Z. Wang, Y. Li, P. Liu, Q. Qi, F. Zhang, G. Lu, X. Zhao and X. Huang, *Nanoscale*, 2019, **11**, 5330–5335.

25 H. Gu, Z. Wang and Y. Hu, *Sensors*, 2012, **12**(5), 5517–5550.